Journal of Materials Chemistry B

Accepted Manuscript

This article can be cited before page numbers have been issued, to do this please use: L. Meng, D. Wang, C. Hou, J. Long, J. Jing, D. Dang, Z. Fei and P. Dyson, *J. Mater. Chem. B*, 2017, DOI: 10.1039/C6TB02755E.

ROYAL SOCIETY OF CHEMISTRY

rsc.li/materials-b

View Article Online
DOI: 10.1039/C6TB02755E

Journal of Material Chemistry B

ARTICLE

Stepwise Growth of Gold Coated Cancer Targeting Carbon Nanotubes for the Precise Delivery of Doxorubicin Combined with Photothermal Therapy

Received 00th october 2016,
Accepted 00th December 2016

DOI: 10.1039/x0xx00000x

www.rsc.org/

Daquan Wang [a,1], Chen Hou[b,1], Lingjie Meng[a*], Jiangang Long[b], Jiange Jing[a], Dongfeng Dang[a], Zhaofu Fei[c], Paul J. Dyson[c*]

Combining doxorubicin with thermal therapy in the clinic has led to startling results in the treatment of problematic cancers. Here, we describe a multimodal multi-walled carbon nanotube material that combines tumor targeting, doxorubicin delivery, and photothermal therapy for localized cancer treatment. The agent was constructed layer-by-layer from polypyrrole and gold nanoparticles on multi-walled carbon nanotubes. The gold surface was modified with tumor targeting folic acid terminated PEGylated chains, which also provide water-dispersibility, biocompatibility and should extend the half-life in blood. The material has a high loading/unloading capacity for the cytotoxic agent doxorubicin. Release of the doxorubicin, combined with the photothermal properties of the material that induces localized hyperthermia, leads to efficient cancer cell death.

Introduction

Anticancer multimodal therapeutic agents possess unique features that lead to the efficient treatment of cancer with minimal damage to normal tissues and tend to be less prone to drug resistance than other types of chemotherapies.[1, 2] Chemotherapy is one of the most commonly used modalities in cancer treatment, however, the most frequently used anticancer drugs are non-selective compounds which exhibit serious side-effects. As such, tumor targeting drug delivery systems have been developed to improve the therapeutic effect of common chemotherapeutics,[3, 4] although fully overcoming drug-resistance remains challenging.[5, 6] One way to improve the efficacy of a drug is to combine chemotherapy with radiotherapy and such combined therapies are widely employed in the clinic.[7] In addition, there are currently several on-going clinical studies in which chemotherapy is combined with localized heating of a tumor (thermal therapy), to reverse drug resistance.[8] Indeed, doxorubicin (DOX) and macromolecular formulations of DOX are particularly effective when combined with thermal therapy.[9]

Photothermal therapy (PTT) is an alternative approach where light, usually near-infrared (NIR), is converted to heat by a photosensitizer.[10] The method may be viewed as a special type of photodynamic therapy, a clinically used approach, and consequently methods to deliver infrared radiation to cancer sites are well established.[11] Moreover, unlike conventional photodynamic therapy, oxygen is not required and, therefore, PTT can be effective in hypoxic tumors. Like photodynamic therapy, combining the treatment with chemotherapy is often advantageous.[12]

PTT usually employs NIR laser photoabsorbers to generate heat that ablates cancer cells (NIR is preferred as it can penetrate skin and tissues to a reasonable depth).[8] The photoabsorber should have a high photothermal conversation efficiency, low toxicity and good biocompatibility, *i.e.* appropriate size and surface properties to prolong circulation in the blood. Since photoabsorbers are based on nanodimensional materials they have an intrinsic tumor targeting profile due to the enhanced permeability and retention effect.[11] However, incorporating tumor-targeting groups on surface of the photoabsorber can further enhance selective uptake at the tumor site.[9] It has also been shown that loading known anticancer-drugs onto the photoabsorbers can improve the overall efficacy of the system and a number of promising multifunctional photoabsorbers have been reported. These multimodal agents are derived from 2D nanosheets such as graphene oxides (GO),[13, 14] molybdenum disulfide[15]

[a] School of Science, State Key Laboratory for Mechanical Behavior of Materials and MOE Key Laboratory for Nonequilibrium Synthesis and Modulation of Condensed Matter, Xi'an Jiaotong University, Xi'an 710049, P. R. China.
[b] Center for Mitochondrial Biology and Medicine, Ministry of Education Key Laboratory of Biomedical Information Engineering, School of Life Science and Technology, Xi'an Jiaotong University, Xi'an 710049, P. R. China.
[c] Institut des Sciences et Ingénierie Chimiques, Ecole Polytechnique Fédérale de Lausanne (EPFL), 1015 Lausanne, Switzerland.
*E-mail: menglingjie@mail.xjtu.edu.cn
[1] These authors contributed equally.
Electronic Supplementary Information (ESI) available: The size distribution of adsorbed Au NPs; IR,UV-vis and Raman spectra; Combination chemotherapy and photothermal therapy without FA. See DOI:

View Article Online
DOI: 10.1039/C6TB02755E

Journal of Material Chemistry B

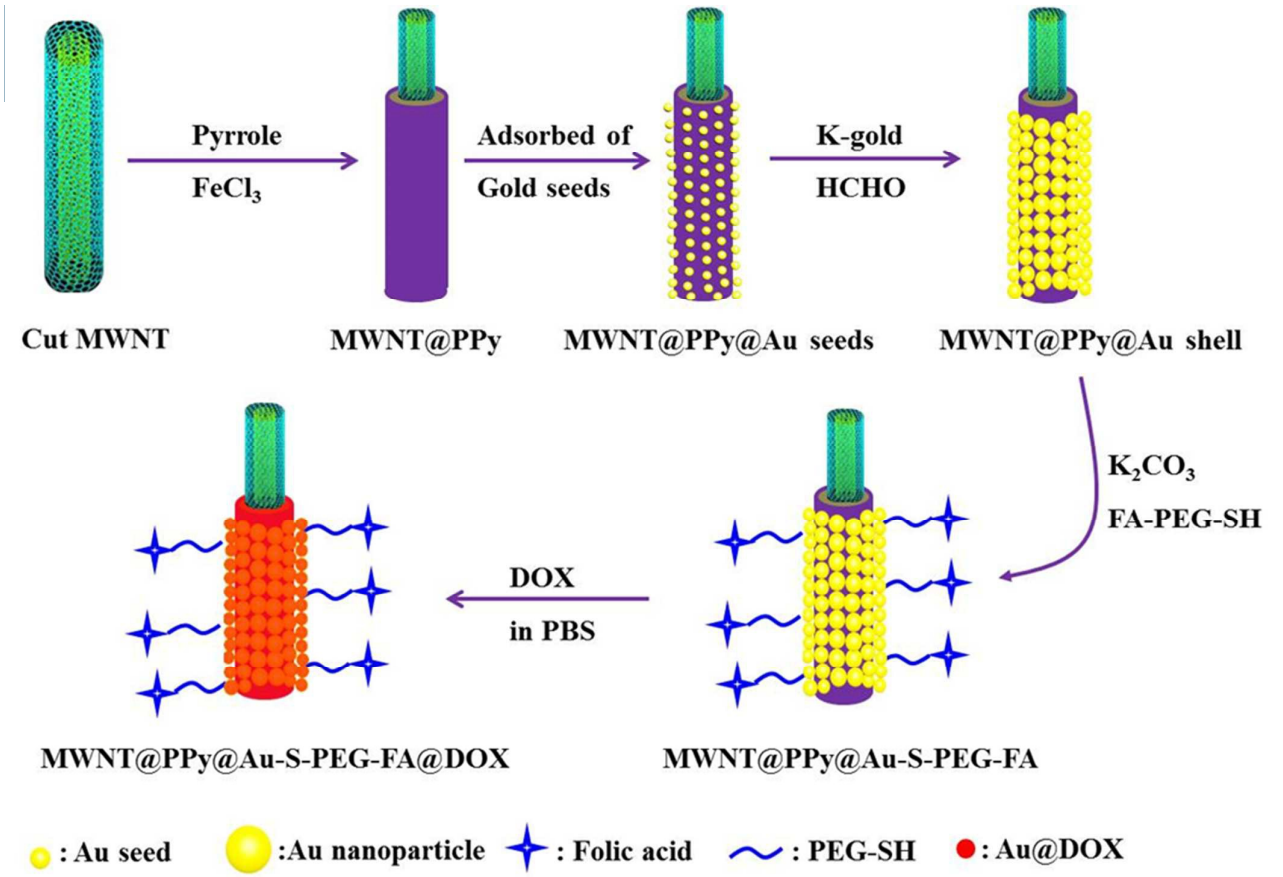

Scheme 1. The route used to prepare the DOX loaded multimodal nanotubes.

and their derivatives,[16, 17] and 0D nanoparticles including Au/Ag nanoparticles,[18-20] carbon nanocapsules,[21] hollow MoO_3 nanospheres[22] and polypyrrole nanocapsules (PPy).[23]

1D nanomaterials, in particular carbon nanotubes (CNTs), have been widely exploited in biomedical applications including drug delivery and PTT because of their large specific area, tubular structure and the capacity to tailor their surface.[24, 25] Both multi-walled carbon nanotubes (MWNTs) and single-walled carbon nanotubes (SWNTs) have emerged as promising drug delivery vehicles due to their remarkable ability to penetrate cell membranes, high drug-loading capacity, and prolonged circulation times in the blood.[26] In addition, carbon nanotubes are also effective PTT agents as they can absorb NIR laser light and convert it into heat.[27, 28] Due to exceptionally high extinction coefficient of gold nanoparticles (Au NPs), it was found that SWNTs coated with noble metal nanoparticles exhibit an enhanced NIR absorption.[29-31]

In this paper, we describe the synthesis of a nanoscale multimodal material based on modified MWNTs empowered with additional tumor targeting properties that can be loaded with high levels of DOX. The resulting composite is highly cytotoxic to cancer cells when applied in combination with photothermal therapy.

Experimental

Materials and method

Carboxylated MWNTs (purity > 95 wt.%, length 1-2μm, diameter 8-15nm) were purchased from Chengdu Organic Chemistry Co., Ltd., China. Cut and oxidized MWNTs were prepared following a literature method.[32] Fetal bovine serum (FBS) and high glucose Dulbecco's Modified Eagle's medium (DMEM) were purchased from Hyclone. WST-1 cell viability assay kit was purchased from Beyotime Biotechnology Co., Ltd. Folate-PEG-SH (M.W. 2000) was purchased from RuiXi Biotechnology Co., Ltd. Pyrrole (99.5%), chloroauric acid trihydrate ($HAuCl_4 \cdot 3H_2O$, Au > 47.5%), sodium borohydride ($NaBH_4$, 98.0%), formaldehyde (37.0%), doxorubicin hydrochloride (DOX, 99.0%) and other reagents were purchased from Aladdin Chemical Reagent Co., Ltd. Au nanoparticles (*av.* diameter 3.5 nm) were prepared according

View Article Online
DOI: 10.1039/C6TB02755E
Journal name ARTICLE

to a modified literature method by reducing $HAuCl_4$ (1 wt.%, 1 mL) in an aqueous solution (100 mL) of $NaBH_4$ (0.008 wt. %) and trisodium citrate (Na_3Ct, 0.2 wt.%) at 4 °C.[33] A potassium-basic solution of gold salt (K-gold solution) was prepared by mixing K_2CO_3 granules with 1 wt.% $HAuCl_4$ stock solution with continuous stirring in the dark for 12 h.[34] Porous poly(vinylidene chloride) (PVDC) membrane was purchased from Xi'an Kequan Instrument Co., Ltd. (diameter 50 mm and 0.22 μm pore size). Ultrapure water (18.2 MΩ·cm^{-1}) was obtained from a Millipore Milli-Q purification system and was used in all the experiments.

Preparation of MWNT@PPy

An aqueous suspension of the cut and oxidized MWNTs (1 mg·mL^{-1}, 30 mL) was diluted to 100 mL with ultra-pure water and then ultrasonicated for 10 min. After addition of pyrrole (62.4 μL) into the suspension, the resulting mixture was stirred vigorously at room temperature for 15 min, and then ferric chloride aqueous solution (20 mg·mL^{-1}, 15 mL) was added dropwise over 1 min. A black suspension formed and the stirring was continued for a further 8 h at room temperature. The PPy coated MWNTs (MWNT@PPy) were collected using an ultrafiltration device (PVDC, Φ: 0.22μm) and washed with water (5×50 mL). The MWNT@PPy material was then re-dispersed in water and diluted to a volume of 90 mL under ultrasound for 30 min to form a stock MWNT@PPy dispersion (1 mg·mL^{-1}).

Preparation of MWNT@PPy@Au

The MWNT@PPy@Au material was prepared using a seed growth method according to a literature protocol.[34] A stock MWNT@PPy dispersion (1 mg·mL^{-1}, 25 mL) was mixed with a freshly prepared Au NP dispersion (100 mL, diameter ~3.5 nm). The resulting mixture was stirred overnight at room temperature and the product isolated by repeated centrifugation (5000 rpm, 8 min) and washing with water to remove unattached Au NPs. The resulting MWNT@PPy@Au(seed) intermediate was re-dispersed in water (100 mL) and mixed with K-gold solution (60 mL, 10 mM), and reduction was accomplished by addition of aqueous formaldehyde solution (2 mL, 2 wt.%) with stirring for 2 h to generate a dark-purple suspension. The resulting MWNT@PPy@Au material was collected and purified by centrifugation and re-dispersion in water (50 mL) two times.

Preparation of MWNT@PPy@Au-S-PEG-FA

The MWNT@PPy@Au dispersion (1 mg·mL^{-1}, 25 mL) was mixed with an aqueous solution of FA-PEG-SH (5 mg·mL^{-1}, 20 mL) under stirring at room temperature for 24 h. The resulting MWNT@PPy@Au-S-PEG-FA material was collected and washed with water by ultracentrifugation to remove unbound FA-PEG-SH and then re-dispersed in water to 1 mg·mL^{-1}.

DOX loading on and release from the modified nanotubes

The MWNT@PPy, MWNT@PPy@Au or MWNT@PPy@Au-S-PEG-FA materials (2 mL, 1 mg·mL^{-1}) and DOX hydrochloride (9 mg) were mixed in a pH 7.4 PBS buffered solution (10 mL) under stirring. The resulting suspensions were stirred for 16 h at room temperature. The products (denoted as MWNT@PPy@DOX, MWNT@PPy@Au@DOX and MWNT@PPy@Au-S-PEG-FA@DOX, respectively) were collected by repeated ultracentrifugation and washing with pH 7.4 PBS buffered solution until the supernatant was color-free. The amount of unabsorbed DOX was determined by measuring the absorbance at 480 nm (the characteristic absorbance of DOX) relative to a calibration curve recorded under the same conditions, allowing the drug loading to be estimated. DOX release from the MWNT@PPy@Au-S-PEG-FA@DOX material (2 mg) was determined by allowing the material to stand at 37 °C in pH 5.5 and 7.4 PBS buffered solutions (4 mL). After different time intervals MWNT@PPy@Au-S-PEG-FA@DOX was collected from the supernatant by centrifugation, and the concentration of released DOX in the supernatant was estimated spectrophotometrically. The reported values were averaged from three measurements.

Characterization

High resolution-transmission electron microscopy (HR-TEM) was conducted on a TEM-2100 electron microscope at 200 kV (JEOL, Japan). TEM samples were prepared by depositing 5 μL of dilute solution on a copper micro-grid (230-mesh) and then drying at ambient temperature prior to analysis. The size and distribution of Au nanoparticles were determined from TEM micrographs using ImageJ (V1.41, NIH, USA). Fourier-transform infrared (FT-IR) spectra were recorded on a Paragon 1000 (Perkin Elmer) spectrometer. Samples were dried overnight at 45 ºC under vacuum and thoroughly mixed and crushed with KBr to fabricate KBr pellets. UV-vis absorption spectra were recorded on a Lambda 20 spectrometer (Perkin Elmer, Inc.). Zeta (ζ) potentials were measured by a Nano ZS90 Zetasizer (Malvern, U.K.). Raman spectra were measured via Raman microscope using an argon ion laser operating at 514 nm (Renishaw, U.K.). The photothermal properties of the modified MWNTs were studied using a NIR laser diode (808 nm, 1.18 W, spot size 0.75 cm^2) and a digital thermometer (accuracy 0.1 °C, OMEGA Engineering Inc.).

Photothermal Conversion Experiments

Aqueous suspensions of the modified MWNTs (1.0 mL, 50 μg·mL^{-1}) were placed in a plastic tube (10 × 10 × 20 mm^3) and exposed to an 808 nm NIR laser source (1.5 W·cm^{-2}) at a distance of 10 cm and the temperature of the solution was measured as a function of time.

Cell culture and cytotoxicity studies

Human HeLa cells and rat H9C2 cardiomyoblasts were obtained from ATCC (Manassas, VA). The cell culture procedure followed a literature method.[34] HeLa and H9C2 cells were grown in DMEM supplemented with 25 mM glucose, 10% fetal bovine serum, 100 U·mL^{-1} penicillin G sodium, and 100 μg ·mL^{-1} streptomycin sulfate in 10 cm^2 plates at 37 °C in 5% CO_2. For cells incubated with modified MWNTs, the cells seeded in 96-well plates at a density of 5×10^4 per well, After 24 h, cells were washed with FBS-free DMEM and then incubated with modified MWNTs (0, 10, 25, 50 and 100 μg·mL^{-1}) at 37 ℃ in FBS-free DMEM for 1 h. The modified MWNT solution was discarded and the cells were washed with PBS and cultured in fresh medium. After 24 h, cell viability was determined by the WST-1 method. [26] The optical densities

View Article Online
DOI: 10.1039/C6TB02755E

were read at 450 nm using a microplate spectrophotometer (Spectra Max 190, Molecular Devices). Cells cultured without modified MWNTs were used as the control.

Photothermal hyperthermia on HeLa and H9C2 cells

HeLa and H9C2 cells were cultured overnight to allow attachment and then washed with FBS-free DMEM and then incubated in fresh FBS-free DMEM (180 mL). A suspension of the modified MWNTs in PBS (20 mL, 500 $\mu g \cdot mL^{-1}$) was then added and the resulting mixture was incubated at 37 °C for 24 h. Before irradiation, the free modified nanotubes were separated from cultured medium by rinsing three times with PBS. The cells were then irradiated with a laser diode (1.5 $W \cdot cm^{-2}$) at a wavelength of 808 nm and at a distance of 10 cm for 8 min. After irradiation, the cells were rinsed three times with PBS and cell viability was assessed by WST-1 assay as described above.

Results and discussion

Preparation of the photothermal material

The layer-by-layer growth route used to prepare the photothermal material (Scheme 1) commences with cut and oxidized MWNTs, [21,26] as these have been shown to possess the optimum biocompatibility for drug delivery. In the first step an aqueous suspension of the cut and oxidized MWNTs was treated with pyrrole (Py), which was then polymerized by the addition of ferric chloride solution to afford PPy coated MWNTs (termed MWNT@PPy). PPy could improve the photothermal conversation efficiency of the MWNTs due to their excellent NIR absorption capacity[23], and should also facilitate attachment of the Au nanoparticles via complementary electrostatic interaction. A gold layer was then grown on the MWNT@PPy material using a seed growth method.[27] Au seeds of *ca.* 3.5 nm diameter were initially absorbed onto the surface of the MWNTs, which were then treated with formaldehyde (a mild reducing agent that induces seed growth), resulting in the formation of larger, densely packed and integrated Au NPs on the MWNT surfaces affording the MWNT@PPy@Au material.

Gold surfaces are readily functionalized by thiols [31] and, accordingly, folic acid terminated PEGylated chains (FA-PEG-SH) were reacted with the MWNT@PPy@Au material to afford MWNT@PPy@Au-S-PEG-FA. Folic acid is known to accumulate in cancer cells,[35] and is widely used as a cancer targeting group.[36] Moreover PEG has been shown to improve the biocompatibility and water solubility of CNT and can extent the circulation time of nanomedicines in the blood.[26] In the final step the cytotoxic chemotherapeutic agent, DOX, was adsorbed onto the modified MWNTs, presumably via π-π stacking interactions with the PPy.

The structure and morphology of the modified MWNTs were probed by high resolution-transmission electron microscopy (HR-TEM, Fig. 1). The cut and oxidized MWNTs have relatively smooth walls without apparent impurities, and tend to be well separated with lengths generally < 1 μm (Fig. 1A). After coating

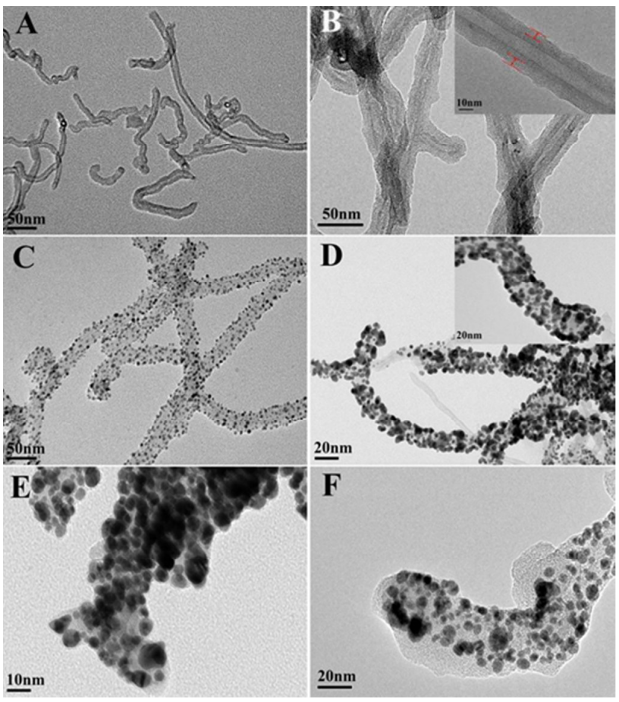

Fig. 1. TEM images of (A) cut and oxidized MWNTs, (B) MWNT@PPy (inset shows a magnified image), (C) MWNT@PPy@Au (seeds), (D) MWNT@PPy@Au (inset shows a magnified image), (E) MWNT@PPy@Au-S-PEG-FA and (F) MWNT@PPy@Au-S-PEG-FA@DOX.

with PPy, the core-shell structures of the MWNT@PPy material can be clearly observed due to the difference in contrast between the polymer and the MWNTs (Fig. 1B). The thickness of the PPy layer is estimated to be about 9 nm. TEM shows that the Au seeds are uniformly spread over the surface of the MWNT@PPy material (Fig. 1C), with the diameter of Au seeds ranging from 2 to 6 nm (ESI, Fig. S1a). After the seed-growth process, the size of Au NPs increased to 6-16 nm (ESI, Fig. S1b), with the NPs often connected each other to form a type of Au exoskeleton around the MWNT@PPy core (Fig. 1D). Following derivatization with FA-PEG-SH, the appearance of the MWNT@PPy@Au-S-PEG-FA material differs to that of its precursor by the presence of a thin (gray) layer presumably corresponding to the PEG-FA coating (Fig. 1E). Finally, in the DOX loaded system a thick gray layer is observed around the MWNT@PPy@Au-S-PEG-FA material (Fig. 1F), indicating that a large amount of DOX has been adsorbed on the modified MWNTs.[37]

The formation of PPy was confirmed by FT-IR spectroscopy (ESI, Fig. S2). The IR spectrum of the MWNTs exhibit characteristic peaks corresponding to O-H, C=O and C-O stretches at 3433, 1716, and 1134 cm^{-1}, respectively, indicative of the presence of -OH and COOH groups following cutting and oxidation. After coating with the PPy layer, vibrations at 3143, 3030, 1546, 1310, 1190 and 1047 cm^{-1} are observed which may be assigned to the PPy polymer.[38, 39]

DOI: 10.1039/C6TB02755E

The presence of both the FA-PEGylated chains and DOX was corroborated by UV-vis spectroscopy (ESI, Fig. S3). The UV-vis spectra of folic acid and DOX contain strong absorptions at 290 and 480 nm, respectively, and the spectrum of the MWNT@PPy@Au-S-PEG-FA@DOX composite contains peaks at similar wavenumbers. The absorption peaks corresponding to DOX on the MWNT@PPy@Au-S-PEG-FA material are red-shifted, indicative of interactions between DOX and the MWNT@PPy@Au-S-PEG-FA nanomaterial. In addition, a peak at 530 nm is characteristic of Au NPs.[40]

The interactions between the MWNTs, PPy layer and Au NPs were probed by Raman spectroscopy (ESI, Fig. S4). The MWNTs, MWNT@PPy, MWNT@PPy@Au and MWNT@PPy@Au-S-PEG-FA samples show three distinct peaks at *ca.* 1348 cm^{-1} (D band), 1576 cm^{-1} (G band) and 2689 cm^{-1} (2D band). The D band arises from the absorption of the amorphous carbon and the defective graphite structure, whereas the G and 2D bands may be attributed to the sp^2 hybridized carbon atoms in highly crystalline graphite.[41] Therefore, the relative intensity ratio of the D band to the G band (*i.e.*, I_D/I_G) reflects the extent of the defects in the MWNTs. The (I_D/I_G) value for the MWNT, MWNT@PPy, MWNT@PPy@Au and MWNT@PPy@Au-S-PEG-FA materials are estimated to be 1.02, 0.90, 0.91 and 0.97, respectively. The I_D/I_G ratio of the PPy coated MWNT decreases, indicating the PPy may coat the MWNTs in an ordered fashion and reduce the disordering of the MWNT surfaces.[42] After application of the Au NPs to the MWNT@PPy material the I_D/I_G ratio remains unchanged (ESI, Fig. S4), suggesting that the generation of the Au layer does not impact on the structure of the MWNTs.

The surface (ζ) potential of the MWNTs is -13.6 ± 0.3 mV and increases to 53.8 ± 2.6 mV after being coated with PPy (Table 1). The negative ζ potential of the MWNT@PPy@Au material (-35.8 ± 1.4 mV) may be attributed to the negatively charged Au NPs, suggesting that the PPy layer plays a key role bridging the negatively charged MWNTs with anionic carboxylate groups and the negatively charged Au NPs. The organic FA-PEG-chains in the MWNT@PPy@Au-S-PEG-FA material insulates the charge to some extent as the ζ potential increases to -20.7±1.1 mV. Following adsorption of positively charged DOX onto the modified MWNTs, the ζ potential increased further to 30.4 ± 1.3 mV.

DOX loading/unloading on the modified nanotubes and their photothermal properties

The DOX loading ratio on the MWNT@PPy, MWNT@PPy@Au and MWNT@PPy@Au-S-PEG-FA materials was quantified by UV-vis spectroscopy, and corresponds to 410, 422 and 432%, respectively (Fig. 2A). These values are in the upper range reported for carbon nanotubes (100-400%),[43] in which the DOX adheres to carbon nanotubes via π-π interactions.[44] The release of DOX from the modified MWNTs was monitored by UV-vis spectroscopy as a function of pH.

Table. 1 ζ potential of the modified MWNTs.

Sample	ζ potential (mV, 25℃)[a]
Cut MWNT	-13.6± 0.3
MWNT@PPy	53.8 ± 2.6
MWNT@PPy@Au	-35.8± 1.4
MWNT@PPy@Au-S-PEG-FA	-20.7 ± 1.1
MWNT@PPy@Au-S-PEG-FA@DOX	30.4 ± 1.3

[a]Values are averaged from three measurements

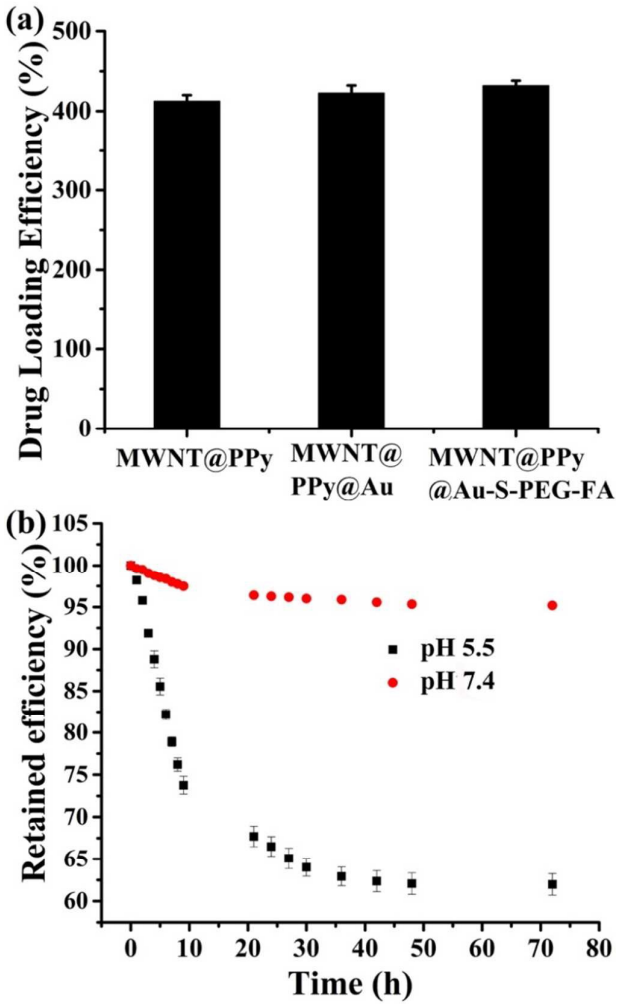

Fig. 2 (A) DOX loading efficiency of the MWNT@PPy, MWNT@PPy@Au and MWNT@PPy@Au-S-PEG-FA. (B) Controlled DOX release from the MWNT@PPy@Au-S-PEG-FA@DOX material in 0.01 M PBS, red: pH 7.4; black: pH 5.5 (the error bars for the data at pH 7.4 are too short to show, SD < 0.25%).

The drug release curves (Fig. 2B) show that DOX is well retained at pH 7.4 at 37 °C in the MWNT@PPy@Au-S-PEG-FA@DOX material, with only 5% of the DOX being released over 72 hours. In contrast, at pH 5.5 more than 25% of the DOX was released within 10 h and over the following 62 h a further 15% of the DOX is gradually released. The show

View Article Online
DOI: 10.1039/C6TB02755E

release of DOX could potentially enhance the cytotoxic effect of the compound,[45, 46] and should be facilitated in the low pH micro-environments of intracellular lysosomes and endosomes or hypoxic cancerous tissue more generally.[43]

The MWNT and MWNT@PPy materials do not exhibit any significant absorptions between 400-900 nm. In contrast, the UV-vis spectra of the MWNT@PPy@Au and MWNT@PPy@Au-S-PEG-FA materials exhibit a peak at *ca.* 545 nm, presumably emanating from interactions between the Au NPs and between the Au NPs and MWNT surface. Subsequently, the photothermal conversion of the modified MWNTs was studied, by irradiation with a laser (808 nm) at different powers employing a thermocouple digital thermometer to monitor the temperature change of the solution in real time (Fig. 3A).[47] As expected from the UV-vis spectra, all the modified MWNT suspensions lead to a similar increase in temperature during the course of the experiment.[48] The photothermal conversion capacity of the MWNT@PPy@Au-S-PEG-FA material is slightly reduced due to the shielding effect of the FA-PEG coating. [49, 50] The temperature increase is dependent on the concentration of the sample and the laser power (Fig. 3B). For example, a 50 μg·mL^{-1} suspension of the MWNT@PPy@Au-S-PEG-FA material heats from 25 °C to 45 °C in 8 min under a laser power of 1.5 W·cm^{-2} and this temperature is sufficient to induce cancer cell death.[37]

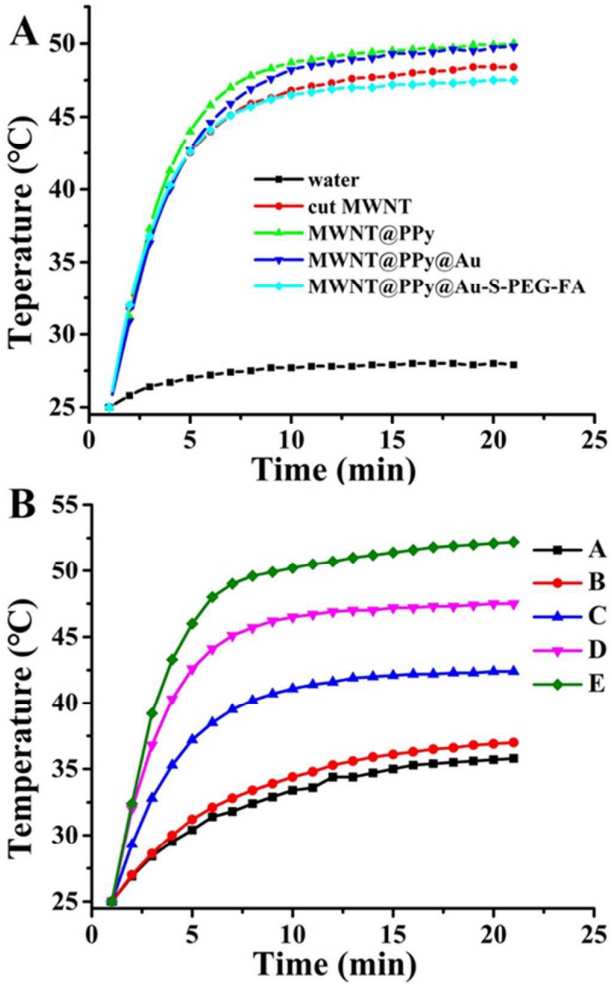

Fig. 3 (A) Photothermal conversation curves of the modified MWNTs (50 μg·mL^{-1})exposed to an 808 nm laser of 1.5 W·cm^{-2}. (B) Influence of the concentration of MWNT@PPy@Au-S-PEG-FA and laser power on the photothermal effect: **A:** 50 μg·mL^{-1} under 0.5 W·cm^{-2}; **B:** 20 μg·mL^{-1} under 1.5 W·cm^{-2}; **C:** 50 μg·mL^{-1} under 1.0 W·cm^{-2};**D:** 50 μg·mL^{-1} under 1.5 W·cm^{-2}; **E:** 100 μg·mL^{-1} under 1.5 W·cm^{-2}.

Biocompatibility of the MWNT@PPy@Au -S-PEG-FA material and combination therapy using the MWNT@PPy@Au-S-PEG-FA@DOX system

The cytotoxicity of the MWNT and MWNT@PPy@Au-S-PEG-FA materials were assessed using the WST-1 assay in rat H9C2 cardiomyoblasts and human HeLa cells (Fig. 4). Both materials showed limited damage to the two cell lines in the concentration range of 0 - 100 μg·mL^{-1} after incubation for 24 h. Indeed, cell death was not observed at a dose of 25 μg·mL^{-1} for the MWNT@PPy@Au-S-PEG-FA material illustrating the viability of this material as a drug delivery material for PTT.

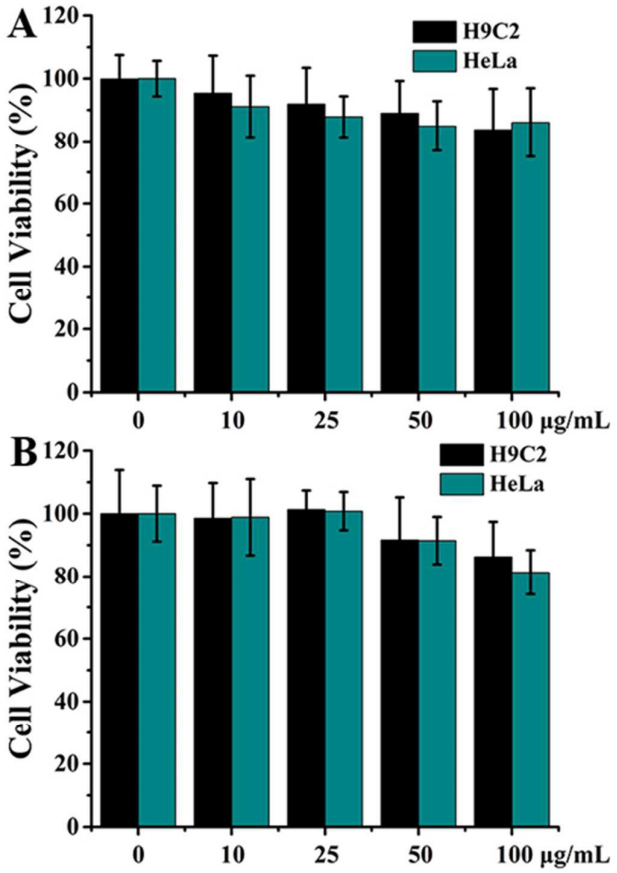

Fig. 4 Cell viability of H9C2 and HeLa cells after incubation with the (A) MWNT and (B) MWNT@PPy@Au-S-PEG-FA materials as a function of concentration over 24 h.

View Article Online
DOI: 10.1039/C6TB02755E

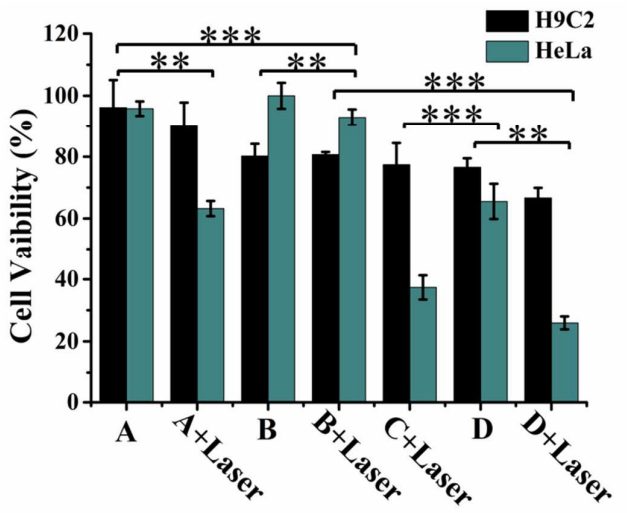

Fig. 5 Combination chemotherapy and photothermal therapy on H9C2 and HeLa cells after incubating with A: cut MWNT, B: DOX, C: MWNT@PPy@Au-S-PEG-FA, D: MWNT@PPy@Au-S-PEG-FA@DOX at 50 $\mu g \cdot mL^{-1}$ for 24 h or then irradiated using an 808 nm laser at 1.5$W \cdot cm^{-2}$ for 8 min. $^{*}P<0.05$, $^{**}P<0.01$, and $^{***}P<0.001$.

The MWNT@PPy@Au-S-PEG-FA and MWNT@PPy@Au-S-PEG-FA@DOX materials were evaluated in combination with PTT in the H9C2 and HeLa cells, with cut MWNT and DOX also studied as controls. As expected, the MWNTs and DOX show negligible toxicity to the two cell lines, whereas the combination of the modified MWNTs and PTT induces cancer cell death (Fig. 5). Although the cut MWNTs are biocompatible with the H9C2 and HeLa cells, more than 30% of the HeLa cells could be killed by hyperthermia after irradiation by 808 nm laser (note that cancer cells are more sensitive to heat than healthy cells). [51] H9C2 cells were slightly sensitive to DOX whereas the drug has almost no effect on HeLa cell under the test conditions. The MWNT@PPy@Au-S-PEG-FA material is essentially non-toxic to the two cancer cell lines (Fig. 4). However, when the MWNT@PPy@Au-S-PEG-FA material is used in combination with a laser (808 nm), some cytotoxicity is observed in the H9C2 cell line and high cytotoxicity is observed in the HeLa cells (only 37% of HeLa cells survive, *i.e.* the IC_{50} value is surpassed). With the DOX loaded material, *i.e.* MWNT@PPy@Au-S-PEG-FA@DOX, moderate cytotoxicity was observed in the absence of light (76 and 65% cell survival in the H9C2 and HeLa cells, respectively), whereas when applied at the same dose in combination with PTT, cell death increases substantially. In the HeLa cell line only 26% cell survival is observed, indicating the synergy between the two therapeutic regimes. Note, the assay was performed such that the modified MWNT medium was discarded prior to irradiation, indicating that the photothermal enhancement arises from material taken into the cells.

It is noteworthy that these materials are systematically more cytotoxic to the HeLa cell line as this cell line contains excess folate receptors (whereas H9C2 cells do not), which implies the FA-targeting groups play a crucial role.[52] To assess the targeting property of FA, related materials without FA were prepared and evaluated, *i.e.* MWNT@PPy@Au-S-PEG and MWNT@PPy@Au-S-PEG@DOX (Fig. S5). These materials are slightly more active on the H9C2 cells and less cytotoxic to the HeLa cells, which supports the role of FA targeting in the latter cell line where the FA receptors are overexpressed.

Conclusions

A high-performance multimodal therapeutic nanoscale drug delivery system that combines targeted chemotherapy and photothermal therapy has been developed. The exoskeletal-like gold layer has only a modest impact on the photothermal conversion of the material, but importantly allows FA terminated PEG chains to be covalently attached to the surface of the material via a sulfide group. The DOX loaded tumor targeting material is biocompatible and disperses well in water. It has been shown that the resulting MWNT@PPy@Au-S-PEG-FA@DOX exhibits effective hyperthermia and rapid drug release at low pH resulting in efficient cancer cell death. The nanomedicine is endowed with cancer cell selectivity, *i.e.* to cancer cells that overexpress FA receptors. Such a system could prove to be beneficial to overcome drug resistance cancers.

Acknowledgements

This work was supported by the National Natural Science Foundation of China (21474079, 21674085), the Program for New Century Excellent Talents in University (NCET-13-0453), and the Fundamental Funds for the Central Universities (08143101). We also thank Mr Chuansheng Ma, and Mr Yanzhu Dai from International Center for Dielectric Research (ICDR), Xi'an Jiaotong University for their assistance with TEM analysis.

Notes and references

1 B. Jang, H. Kwon, P. Katila, S. J. Lee and H. Lee, Adv. Drug Deliver. Rev., 2016, 98, 113-133.
2 F. Rozet, F. Audenet, R. Sanchez-Salas, M. Galiano, E. Barret and X. Cathelineau, Expert. Rev. Anticanc., 2013, 13, 811-818.
3 T. M. Allen and P. R. Cullis, Adv. Drug Deliver. Rev., 2013, 65, 36-48.
4 P. T. Wong and S. K. Choi, Chem. Rev., 2015, 115, 3388-3432.
5 R. Perez-Tomas, Curr. Med. Chem., 2006, 13, 1859-1876.
6 A. Singh and J. Settleman, Oncogene, 2010, 29, 4741-4751.
7 I. Bozic, J. G. Reiter, B. Allen, T. Antal, K. Chatterjee, P. Shah, Y. S. Moon, A. Yaqubie, N. Kelly, D. T. Le, E. J. Lipson, P. B. Chapman, L. A. Diaz, Jr., B. Vogelstein and M. A. Nowak, eLife, 2013, 2, e00747.
8 L. Zou, H. Wang, B. He, L. Zeng, T. Tan, H. Cao, X. He, Z. Zhang, S. Guo and Y. Li, Theranostics, 2016, 6, 762-772.
9 G. Modugno, C. Menard-Moyon, M. Prato and A. Bianco, Brit. J. Pharmacol., 2015, 172, 975-991.
10 Z. H. Bao, X. R. Liu, Y. D. Liu, H. Z. Liu and K. Zhao, Asian. J. Pharm. Sci., 2016, 11, 349-364.

View Article Online
DOI: 10.1039/C6TB02755E

11 L. Cheng, C. Wang, L. Feng, K. Yang and Z. Liu, Chem. Rev., 2014, 114, 10869-10939.
12 C. He, X. Duan, N. Guo, C. Chan, C. Poon, R. R. Weichselbaum and W. Lin, Nat. commun., 2016, 7, 12499.
13 R. K. Thapa, J. Y. Choi, B. K. Poudel, H. G. Choi, C. S. Yong and J. O. Kim, Int. J.Nanomedicine., 2016, 11, 2799-2813.
14 W. Zhang, Z. Y. Guo, D. Q. Huang, Z. M. Liu, X. Guo and H. Q. Zhong, Biomaterials, 2011, 32, 8555-8561.
15 W. Y. Yin, L. Yan, J. Yu, G. Tian, L. J. Zhou, X. P. Zheng, X. Zhang, Y. Yong, J. Li, Z. J. Gu and Y. L. Zhao, Acs Nano, 2014, 8, 6922-6933.
16 X. X. Ma, H. Q. Tao, K. Yang, L. Z. Feng, L. Cheng, X. Z. Shi, Y. G. Li, L. Guo and Z. Liu, Nano Res., 2012, 5, 199-212.
17 J. J. Shi, L. Wang, J. Zhang, R. Ma, J. Gao, Y. Liu, C. F. Zhang and Z. Z. Zhang, Biomaterials, 2014, 35, 5847-5861.
18 Z. L. Jiang, B. Dong, B. T. Chen, J. Wang, L. Xu, S. Zhang and H. W. Song, Small, 2013, 9, 604-612.
19 H. Y. Liu, D. Chen, L. L. Li, T. L. Liu, L. F. Tan, X. L. Wu and F. Q. Tang, Angew. Chem. Int. Ed., 2011, 50, 891-895.
20 X. J. Wu, L. Z. Zhou, Y. Su and C. M. Dong, Biomacromolecules, 2016, 17, 2489-2501.
21 H. Wang, Y. B. Sun, J. H. Yi, J. P. Fu, J. Di, A. D. Alonso and S. Q. Zhou, Biomaterials, 2015, 53, 117-126.
22 T. Bao, W. Y. Yin, X. P. Zheng, X. Zhang, J. Yu, X. H. Dong, Y. Yong, F. P. Gao, L. Yan, Z. J. Gu and Y. L. Zhao, Biomaterials, 2016, 76, 11-24.
23 Y. Wang, Y. Xiao and R. K. Tang, Chem. Eur. J., 2014, 20, 11826-11834.
24 Z. Liu, S. Tabakman, K. Welsher and H. J. Dai, Nano Res., 2009, 2, 85-120.
25 S. Vardharajula, S. Z. Ali, P. M. Tiwari, E. Eroglu, K. Vig, V. A. Dennis and S. R. Singh, Int. J. Nanomedicine., 2012, 7, 5361-5374.
26 L. Meng, X. Zhang, Q. Lu, Z. Fei and P. J. Dyson, Biomaterials, 2012, 33, 1689-1698.
27 H. K. Moon, S. H. Lee and H. C. Choi, Acs Nano, 2009, 3, 3707-3713.
28 F. F. Zhou, D. Xing, Z. M. Ou, B. Y. Wu, D. E. Resasco and W. R. Chen, J. Biomed. Opt., 2009, 14.
29 L. J. Meng, L. Y. Niu, L. Li, Q. H. Lu, Z. F. Fei and P. J. Dyson, Chem. Eur. J., 2012, 18, 13314-13319.
30 L. J. Meng, W. J. Xia, L. Liu, L. Y. Niu and Q. H. Lu, ACS Appl. Mater. Interfaces, 2014, 6, 4989-4996.
31 X. J. Wang, C. Wang, L. Cheng, S. T. Lee and Z. Liu, J. Am. Chem. Soc., 2012, 134, 7414-7422.
32 Z. Y. Chen, K. Kobashi, U. Rauwald, R. Booker, H. Fan, W. F. Hwang and J. M. Tour, J. Am. Chem. Soc., 2006, 128, 10568-10571.
33 W. Chen, H. H. Deng, L. Hong, Z. Q. Wu, S. Wang, A. L. Liu, X. H. Lin and X. H. Xia, Analyst, 2012, 137, 5382-5386.
34 L. Meng, W. Xia, L. Liu, L. Niu and Q. Lu, ACS Appl. Mater. Interfaces, 2014, 6, 4989-4996.
35 Garin-Chesa Pilar, Patricia E. Saigo, Jojn L.Lewis, Jr., Lioyd J. Old, and Wolfgang J.Retting, Am. J. Patbol., 1993, 142, 557-567.
36 J. Sudimack and R. J. Lee, Adv. Drug Deliver. Rev., 2000, 41, 147-162.
37 D. Jaque, L. Martinez Maestro, B. del Rosal, P. Haro-Gonzalez, A. Benayas, J. L. Plaza, E. Martin Rodriguez and J. Garcia Sole, Nanoscale, 2014, 6, 9494-9530.
38 Y. Yu, C. Ouyang, Y. Gao, Z. Si, W. Chen, Z. Wang and G. Xue, J. Polym. Sci. Polym. Chem., 2005, 43, 6105-6115.
39 Y.-S. Chen, Y. Li, H.-C. Wang and M.-J. Yang, Carbon, 2007, 45, 357-363.
40 N. G. Bastus, J. Comenge and V. Puntes, Langmuir, 2011, 27, 11098-11105.
41 L. Bokobza, Express. Polym. Lett., 2012, 6, 601-608.
42 Y. Fang, J. Liu, D. J. Yu, J. P. Wicksted, K. Kalkan, C. O. Topal, B. N. Flanders, J. Wu and J. Li, J. Power Sources, 2010, 195, 674-679.
43 X. Zhang, L. Meng, Q. Lu, Z. Fei and P. J. Dyson, Biomaterials, 2009, 30, 6041-6047.
44 Y. X. Wang and Z. F. Xu, Rsc Adv., 2016, 6, 314-322.
45 J. Liu, C. Wang, X. Wang, X. Wang, L. Cheng, Y. Li and Z. Liu, Adv. Funct. Mater., 2015, 25, 384-392.
46 M. Zhou, S. Liu, Y. Jiang, H. Ma, M. Shi, Q. Wang, W. Zhong, W. Liao and M. M. Q. Xing, Adv. Funct. Mater., 2015, 25, 4730-4739.
47 L. Meng, L. Niu, L. Li, Q. Lu, Z. Fei and P. J. Dyson, Chem. Eur. J., 2012, 18, 13314-13319.
48 J. W. Fisher, S. Sarkar, C. F. Buchanan, C. S. Szot, J. Whitney, H. C. Hatcher, S. V. Torti, C. G. Rylander and M. N. Rylander, Cancer Res., 2010, 70, 9855-9864.
49 S. Zeng, D. Baillargeat, H. P. Ho and K. T. Yong, Chem. Soc. Rev., 2014, 43, 3426-3452.
50 S. Zeng, X. Yu, W.-C. Law, Y. Zhang, R. Hu, X.-Q. Dinh, H.-P. Ho and K.-T. Yong, Sens Actuat. B-chem, 2013, 176, 1128-1133.
51 C. M. Clavel, P. Nowak-Sliwinska, E. Păunescu, P. J. Dyson, Med. Chem. Commun., 2015, 6, 2054 – 2062.
52 P.S. Low, W. A. Henne, D.D. Doorneweerd , Acc. Chem. Res., 2008, 41,120-129.

View Article Online
DOI: 10.1039/C6TB02755E

TOC